# Structure of Human Adenosine Kinase at 1.5 Å Resolution[†,‡]

Irimpan I. Mathews,[§] Mark D. Erion,[||] and Steven E. Ealick*[,§]

*Department of Chemistry and Chemical Biology, Cornell University, Ithaca, New York 14853, and Metabasis Therapeutics, Inc., 9390 Town Center Drive, San Diego, California 92121*

*Received June 29, 1998; Revised Manuscript Received September 9, 1998*

ABSTRACT: Adenosine kinase (AK) is a key enzyme in the regulation of extracellular adenosine and intracellular adenylate levels. Inhibitors of adenosine kinase elevate adenosine to levels that activate nearby adenosine receptors and produce a wide variety of therapeutically beneficial activities. Accordingly, AK is a promising target for new analgesic, neuroprotective, and cardioprotective agents. We determined the structure of human adenosine kinase by X-ray crystallography using MAD phasing techniques and refined the structure to 1.5 Å resolution. The enzyme structure consisted of one large $\alpha/\beta$ domain with nine $\beta$-strands, eight $\alpha$-helices, and one small $\alpha/\beta$-domain with five $\beta$-strands and two $\alpha$-helices. The active site is formed along the edge of the $\beta$-sheet in the large domain while the small domain acts as a lid to cover the upper face of the active site. The overall structure is similar to the recently reported structure of ribokinase from *Escherichia coli* [Sigrell et al. (1998) *Structure 6*, 183−193]. The structure of ribokinase was determined at 1.8 Å resolution and represents the first structure of a new family of carbohydrate kinases. Two molecules of adenosine were present in the AK crystal structure with one adenosine molecule located in a site that matches the ribose site in ribokinase and probably represents the substrate-binding site. The second adenosine site overlaps the ADP site in ribokinase and probably represents the ATP site. A $Mg^{2+}$ ion binding site is observed in a trough between the two adenosine sites. The structure of the active site is consistent with the observed substrate specificity. The active-site model suggests that Asp300 is an important catalytic residue involved in the deprotonation of the 5′-hydroxyl during the phosphate transfer.

Adenosine kinase (ATP, adenosine 5′-phosphotransferase, EC 2.7.1.20) catalyzes the phosphorylation of ribofuranosyl-containing nucleoside analogues at the 5′-hydroxyl using ATP or GTP as the phosphate donor. Tissue distribution studies indicate that adenosine kinase (AK) is the most abundant nucleoside kinase in mammals with AK activity in humans and monkeys expressed at the highest levels in liver, kidney, and lung and at intermediate levels in the brain, heart, and skeletal muscle (*1*, *2*). AK exhibits a relatively broad substrate specificity tolerating modifications in both the sugar and base moieties (*3*). Accordingly, numerous nucleoside antiviral and anticancer drugs are AK substrates and consequently undergo rapid phosphorylation in vivo to the 5′-monophosphate. In many cases, the monophosphate is subsequently converted by other kinases to the triphosphate which functions as the active metabolite. Examples include ribavirin (*4*) and mizoribine (*5*).

The physiological function of AK is associated with the regulation of extracellular adenosine levels and the preservation of intracellular adenylate pools (*6*). Adenosine is a locally acting hormone produced from the breakdown of intracellular ATP pools primarily to preserve tissue function during times of ischemia or cellular stress (*7*, *8*). Adenosine activates one or more of the four adenosine receptor subtypes and thereby elicits a diverse array of pharmacological responses dependent on the cell type and tissue expressing the receptor. Steady-state levels of adenosine are controlled by AK, 5′-nucleotidase, and adenosine deaminase. On the basis of its lower $K_M$, AK is believed to be the primary route of adenosine metabolism and inhibitors of AK are therefore expected to produce a substantial elevation in adenosine levels. In vivo, AK inhibitors exhibit good efficacy in animal models of stroke (*9*), seizure (*10*), pain (*11*), and inflammation (*12*). These studies further indicate that AK inhibitors, unlike adenosine receptor agonists, produce the pharmacological benefit without simultaneously evoking hemodynamic effects.

Some biochemical and structural features of AK were reported in studies using enzyme purified from yeast (*13*), *Leischmania donovani* (*14*), rat liver (*15*), rat brain (*16*), murine leukemia L1210 cells (*17*), rabbit liver (*3*), human liver (*6*), human erythrocytes, and human placenta (*14*). More recently, human AK was purified to homogeneity from *Escherichia coli* expressing the AK gene cloned from a human liver cDNA library (*18*). Kinetic studies indicated that AK follows an ordered bi-bi mechanism except for one study which reported a ping-pong mechanism for AK from murine leukemia 1210 cells (*17*). An ordered mechanism proceeding without involvement of a phosphoenzyme intermediate was also consistent with a mechanistic study

[†] This work supported by a National Institutes of Health grant to S.E.E. (RR01646). S.E.E. is indebted to the W. M. Keck Foundation and the Lucille P. Markey Charitable Trust.

[‡] The Brookhaven Protein Data Bank code for human adenosine kinase is 1BX4.

* Corresponding author. Phone: (607) 255-7961. Fax: (607) 255-4137. E-mail: see3@cornell.edu.

[§] Cornell University.

[||] Metabasis Therapeutics, Inc.

10.1021/bi9815445 CCC: $15.00 
Published on Web 10/22/1998

showing net stereochemical inversion for the phosphoryl transfer (*19*). In contrast, little agreement is found in the literature for the order of substrate binding and product release. Studies with partially purified adenosine kinase from Ehrlich ascites tumor cells identified ATP as the first substrate to bind and AMP as the last product to be released (*20*). Other studies, however, predicted adenosine to be the first substrate to bind (*21*−*24*) while still others predicted ADP to be the last substrate to leave (*15*).

Analysis of AK activity at high adenosine concentration showed significant substrate inhibition. Saturation kinetics suggested two adenosine-binding sites; one with high affinity which corresponded to the catalytic site and one with much lower affinity. The latter site was reported to differ from the triphosphate-binding site based on competition studies and may serve to regulate AK activity during times of ischemia and high adenosine production (*23*, *25*, *26*). Chemical modification studies supported the existence of a second adenosine-binding site distinct from the ATP site. Studies with the yeast enzyme indicated that adenosine stabilized the enzyme from heat inactivation (*13*) and that a highly reactive thiol group was essential for activity (*27*, *28*). Inactivation studies with 5,5′-dithio-bis(2-nitrobenzoic acid) suggested that the thiol group is associated with the second binding site since protection required adenosine concentrations equivalent to the dissociation constant for this site and greater than 20 times the dissociation constant for the catalytic site (*23*).

Studies monitoring tryptophan fluorescence of the bovine enzyme provided the first insights into the AK structure (*29*). Fluorescence was attributed to three tryptophan residues, which were postulated to be buried in the protein based on the low maximal emission wavelength and the large increase in fluorescence quenching induced by acrylamide and iodide for the unfolded protein. ATP binding induced a marked fluorescence quenching and decreased tryptophan accessibility to acrylamide and iodide. These results suggested that either a tryptophan exists in or near the ATP-binding site or that ATP induces a protein conformational change. Fluorescence quenching was also observed with adenosine, but to a lesser extent. No change in tryptophan accessibility to acrylamide was observed at saturating adenosine concentrations suggesting that native AK and AK complexed to adenosine may exist in a protein conformation distinct from AK complexed to ATP.

Here, we report the first X-ray crystal structure of human adenosine kinase. In our crystals, AK is complexed with two adenosine molecules. The structure of AK is similar to ribokinase which was the first example in a new family of carbohydrate kinases (*30*).

## EXPERIMENTAL PROCEDURES

*Protein Purification*. The AK gene was excised from the pET3a plasmid (*18*) using *Nde*I and *Xho*I and spliced into the T7-based expression vector pET28a containing a 5′ sequence encoding a polyhistidine tag. Expression in the *E. coli* strain BL21(DE3) was accomplished by inducing cells with 1 mM IPTG at an $OD_{600}$ of around 6.3 and harvested 22 h after induction. Since most of the AK was in the insoluble pellet as inclusion bodies at higher temperatures, the induction was performed at 22 °C.

In general, the cells were suspended in 10 times w/v of a buffer containing 50 mM sodium phosphate (pH 7.8) and 300 mM NaCl (buffer A). The cells were lysed using two cycles of French press and 3 × 30 pulse sonication. The lysate was then stirred for 2 h with a preequilibrated Ni-NTA agarose resin (Qiagen). After washing the resin with several volumes of the buffer A and buffer A containing 10% glycerol (buffer B), the bound protein was eluted with 5, 10, 20, 60, and 100 mM imidazole in buffer B. AK with the polyhistidine tag eluted between 60 and 100 mM imidazole and was purified by pooling the 60 and 100 mM fractions followed by exchanging the buffer to 10 mM Tris (pH 7.5) containing 1 mM DTT and applying to a DEAE column. The bound protein was eluted with a linear gradient of 1 to 100 mM KCl in the same buffer. AK eluted at approximately 40 mM KCl. Purified AK was then concentrated to 10 mg/mL for crystallization trials. The polyhistidine tag was cleaved by treating with biotinylated thrombin for 22 h. The thrombin was removed using a streptavidin agarose column. The eluant from this column was collected and the elution buffer exchanged to buffer A. This solution was then stirred for 2 h with a preequilibrated Ni-NTA resin, poured onto a column, and washed with buffer A and buffer B, and the AK was eluted with 5 mM imidazole. The purified AK, without the polyhistidine tag, was concentrated to 10 mg/mL and used for crystallization trials. The selenomethionine (SeMet)-incorporated protein used for MAD phasing was expressed using an *E. coli* strain BL834-(DE3) auxotropic for methionine. The purification procedure for the SeMet protein was identical except that 5 mM DTT was added to prevent oxidation of the SeMet residues.

*Crystallization.* Crystals of AK were grown by the vapor diffusion method in hanging drops using AK with the polyhistidine tag removed. Over 3000 crystallization conditions, with and without substrates and inhibitors, were tried in order to produce crystals suitable for X-ray crystallographic studies. Four different crystal forms were identified. One crystal form contained no ligands, one crystal formed contained adenosine, and two of these crystal forms contained adenosine kinase inhibitors. Attempts to crystallize AK with various analogues of ATP and GTP were unsuccessful, further trials are underway. Crystals used in the X-ray analysis contained adenosine and were obtained using a reservoir solution containing 20% PEG 4K, 0.16 M $MgCl_2$, 0.1 M Tris (pH 7.5), or HEPES (pH 7.5). The hanging drops (4−6 $\mu$L) were composed of a 1:1 mixture of protein and the reservoir solution. These crystals belong to space group $P2_12_12$ with unit cell dimension $a = 65.30$ Å, $b = 111.08$ Å, and $c = 49.69$ Å.

*X-ray Data Collection*. The data for the native protein were collected at cryogenic temperature using the Cornell High Energy Synchrotron Source (CHESS) station F1 with $\lambda = 0.93$ Å. All data were measured with an Area Detector Systems Corporation Quantum 4 CCD mosaic detector placed 135 mm from the sample. A total of 100° of data was measured using the oscillation method. Individual frames consisted of a 1° oscillation angle measured for 40 s. The crystal diffracted beyond 1.5 Å resolution and the final data was 98.3% complete to 1.5 Å resolution with an overall $R_{sym}$ of 0.048. The highest resolution shell (1.58−1.50 Å) had an $R_{sym}$ of 0.185 with 91.4% completion. The integration was performed using the program MOSFLM (*31*)

Table 1: Summary of X-ray Diffraction Data

| | native | edge | peak | remote |
|---|---|---|---|---|
| wavelength (Å) | 0.930 | 0.978 99 | 0.978 72 | 0.950 00 |
| resolution (Å) | 1.50 | 2.250 | 2.250 | 2.250 |
| no. of measurements | 259 153 | 99 941 | 99 904 | 80 722 |
| no. of independent reflections | 57 640 | 17 035 | 17 063 | 16 887 |
| completeness of data | | | | |
| overall | 98.3 | 99.0 | 99.0 | 98.6 |
| outermost shell | 91.4 | 98.0 | 97.8 | 98.3 |
| *R* merge (%) | | | | |
| overall | 4.8 | 5.8 | 6.3 | 5.7 |
| outermost shell | 18.5 | 11.1 | 12.9 | 13.5 |

Table 2: MAD Difference Ratios[a]

| | MAD difference ratios (20.0−2.3 Å) | | |
|---|---|---|---|
| wavelength (Å) | edge | peak | remote |
| 0.978 99 (edge) | 0.065 (0.040) | 0.032 | 0.064 |
| 0.978 72 (peak) | | 0.076 (0.042) | 0.051 |
| 0.950 00 (remote) | | | 0.061 (0.041) |

[a] MAD difference ratios are rms($|\Delta F|$)/rms($|F|$), where $|\Delta F|$ is the Bijvoet difference at one wavelength (diagonal elements) or dispersive difference between pairs of wavelengths (off-diagonal elements) and $|F|$ is the average value of the structure factor magnitude. The values in parentheses are ratios for centric reflections, which ideally should be zero. They are indicators of noise in the anomalous scattering signal.

and data scaling and merging were carried out using the CCP4 package (*32*). Details of the data collection statistics are given in Table 1.

The multiple wavelength anomalous diffraction (MAD) data sets were collected at cryogenic temperatures to 2.3 Å resolution on beamline X-12C at the National Synchrotron Light Source. The wavelength for the Se edge was first determined by scanning the X-ray absorption spectrum near the selenium K-edge of the SeMet-incorporated AK crystal. Three wavelengths were selected for data collection corresponding to the maximum $f''$ (peak), the minimum $f'$ (edge), and a reference wavelength (remote) at 0.9500 Å. The data sets were collected using inverse beam geometry. A total of (150 × 3)° of data were measured using a 1° oscillation angle measured for 60 s. The intensity data were processed and scaled with DENZO/SCALEPACK (*33*). Details of the data collection statistics are given in Table 1.

*Analysis of MAD Data and Location of Se Atom Positions.* The unmerged data, output from the SCALEPACK, were processed with the program SORTAV (*34*) to remove outlying observations. The MADSYS suite of programs (*35*, *36*) were used to scale the data (Table 2) and calculate the moduli of the normal structure factors, $|F_A|$ and $|F_T|$ (corresponding to anomalous scattering atoms and the entire structure, respectively) and the phase difference, $(\phi_T - \phi_A)$. The phasing statistics were reliable up to a resolution of 2.3 Å. The shake-and-bake direct methods procedure as implemented in the computer program SnB (*37*) was used to determine the heavy-atom positions. Two methods were used to generate normalized structure factors for SnB. In the first method, the $F_A$ values obtained from the MADSYS suite were processed with the program SORTAV and normalized structure factors were calculated using the program BAYES (Blessing, personal communication). In the second method, data sets for each individual wavelength (edge and peak) were used to calculate anomalous differences which were then converted to *E* values. Data sets were scaled and processed with the programs LOCSCL and LEVY (*38*) and renormalized *E* values derived from the anomalous differences were calculated by the program DIFFE (*39*).

A total of 192 trials of SnB were executed using the 1317 largest *E* values and 2500 triple phase invariants. Eight random positions were used to calculate phases at the beginning of each trial after which the random phases were subjected to 25 cycles of phase refinement. At the end each trial, the eight largest peaks in the *E* map were used to calculate phases which were subjected to two additional cycles of phase refinement. Correct solutions were identified by a sudden decrease in the minimum function after the first few SnB cycles. A final analysis of the minimum function values from the 192 trials showed a bimodal distribution indicating six trials had converged to solutions. Six Se sites were obtained from the SnB program using the anomalous differences. Similar procedures using $F_A$ values revealed only four of the Se sites.

The MAD data were also analyzed using automated Patterson map searching and the computer program SOLVE (*40*). This procedure revealed seven Se sites resulting in a figure of merit of 0.76 for data from 20 to 3.5 Å resolution. The Se sites located with the two methods were consistent except that SOLVE located one additional site.

*Refinement of Se Atom Positions and Phase Calculation.* The refinement of heavy atom parameters was performed by the ASLSQ program of the MADSYS package. Phases were calculated to 2.3 Å resolution using MADABCD and improved by solvent flattening and density modification using the program DM (*32*). The refinement was also repeated with the MLPHARE program (*41*) followed by solvent flattening with DM. Both maps were of excellent quality showing long continuous stretches of main-chain density with clear density for side chains and carbonyl oxygen atoms. The final map, computed with reflections up to 2.3 Å resolution, was used for chain tracing (Figure 1).

*Model Building and Refinement.* Electron density maps were displayed and model coordinates were fitted on an Extreme 2 Silicon Graphics workstation using the interactive program O, version 5.10.2 (*42*). First, $C_\alpha$ atoms were assigned to the skeleton positions, and then a polyalanine model was built by performing a database search to obtain the best-fitting peptide with respect to the $C_\alpha$ positions. Since the maps were computed at 2.3 Å resolution, most of the side chains and carbonyl oxygen atoms were clear. The

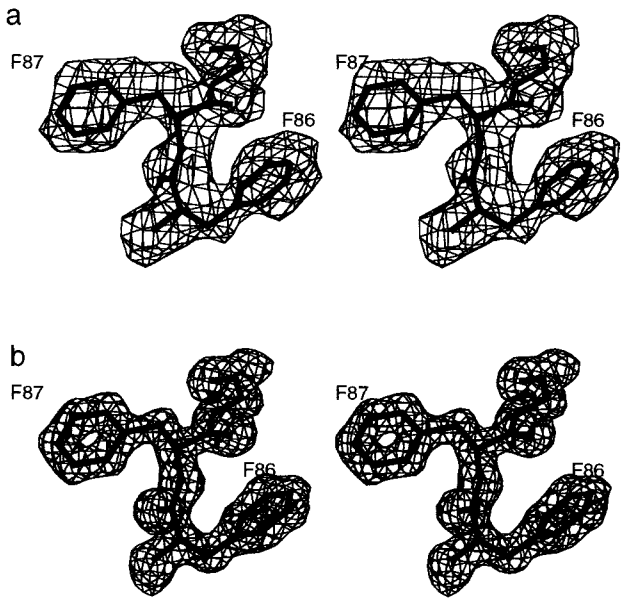


FIGURE 1: Representative portions of the electron density map (contoured at 1$\sigma$). (a) Experimental MAD map calculated at 2.3 Å resolution. (b) The final $2F_o - F_c$ map calculated at 1.5 Å resolution.

model before refinement consisted of 330 residues complete with side chains, except for a few disordered ones.

All model refinement was carried out using the program X-PLOR (*43*). The low resolution cutoff for all refinements was 20.0 A. Reflections with an F/$\sigma$ higher than 2 were used for refinement. After one round of simulated annealing refinement, the *R* factor converged to 28.2% and the $R_{free}$ was 33.0%. Careful examination of the maps allowed corrections to be incorporated into the model. Pro80 was changed to a cis conformation and C-terminal residues from 335 to 345 were included as alanine residues. Another round of refinement showed clear densities for all the side chain except His345.

The resolution of the data was then extended to 1.60 Å. After a few more cycles of manual building, refinement using simulated annealing, and individual *B* factor refinement, the *R* factor and $R_{free}$ had converged to 24.5 and 27.5%, respectively. At this point, two adenosine ligands became clear in the |Fo|-|Fc| electron density maps (Figure 2) and were included in the model. In addition, 150 water molecules were introduced. Subsequent refinement was carried out using the 1.5 Å resolution data. At this stage, from an analysis of the coordination geometry and the temperature factors, three water molecules were changed to $Mg^{2+}$ ions and two water molecules were changed to chloride ions. The *R* factor of the final model is 19.2% ($R_{free}$ = 22.6%), with tightly restrained geometry (Table 3). This model had 342 residues, two adenosine ligands, three $Mg^{2+}$ ions, two chloride ions, and 354 water molecules. The protein model was assessed using the program PROCHECK (*44*). The Ramachandran plot (*45*) showed 90.6% of the residues in the most favored region and 8.4% in the additional allowed region. There are three residues (Gln78, Ser198, and Ala139) in the disallowed region. All three residues have good electron density. The Luzzati plot showed a coordinate error was 0.173 Å for the working set and 0.197 Å for the test set (*46*).

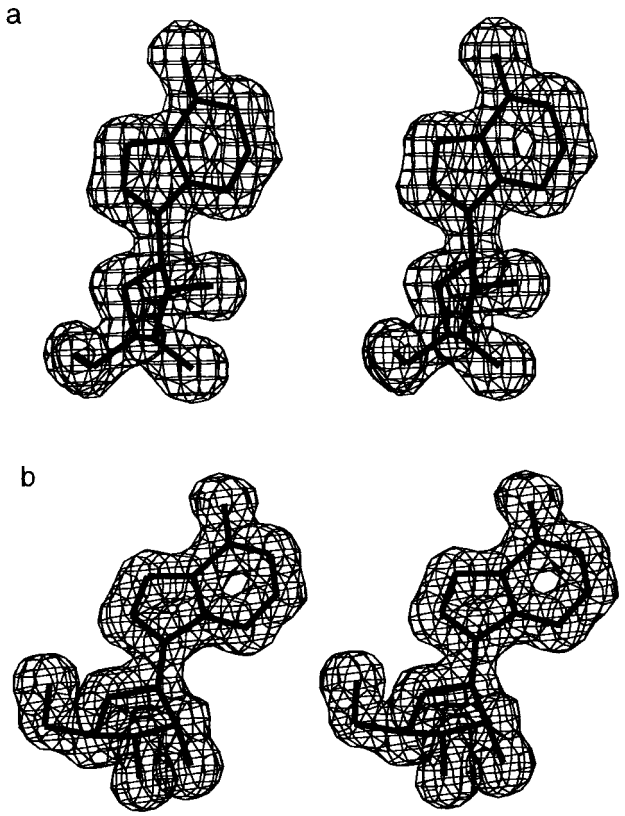


FIGURE 2: Final 1.50 Å resolution electron density maps ($2F_o - F_c$) contoured at 1$\sigma$ for (a) adenosine 1 and (b) adenosine 2.

Table 3: Crystal Data and Refinement Statistics

| | |
|---|---|
| space group | $P2_12_12$ |
| cell dimensions (Å) | |
| *a* | 65.30 |
| *b* | 111.08 |
| *c* | 49.69 |
| *Z* | 4 |
| protein fraction | 0.53 |
| $V_m$ (Å$^3$/Da) | 2.33 |
| resolution limits (Å) | 1.5 |
| no. of protein and ligand atoms | 2734 |
| no. of $Mg^{2+}$ ions | 3 |
| no. of chloride ions | 2 |
| no. of water molecules | 354 |
| *R* factor (%) | 19.2 |
| free *R* factor (%) | 22.6 |
| rms bond (Å) | 0.014 |
| rms angle (deg) | 1.36 |
| rms *B* factor (Å$^2$) | 1.7 |
| av *B* factors (Å$^2$) | |
| main chain atoms | 13.9 |
| side chain | 17.9 |
| ligand atoms | 10.4 |
| adenosine 1 | 9.2 |
| adenosine 2 | 11.6 |
| solvent atoms | 25.3 |

## RESULTS

*Purification and Crystallization.* AK purified by the methods described in the Experimental Section was essentially pure as judged by a Coomassie stained gel. Since the specific activity of AK with and without the polyhistidine tag was similar, crystallization attempts were made with both of the samples. However, diffraction quality crystals were only obtained from the AK with the polyhistidine tag removed. These crystals, grown in the presence of adenos-

ine, belong to the space group $P2_12_12$ with $a = 65.30$ Å, $b = 111.08$ Å, and $c = 49.69$ Å.

*Description of the Overall Structure*. The overall structure of adenosine kinase contains 12 α-helices and 14 β-strands and can be divided into two distinct domains as shown in Figure 3. The structure also contains five segments of $3_{10}$ helix. The larger domain (domain 1) forms an α/β three layer sandwich while the smaller domain (domain 2) forms an α/β two layer structure. The overall dimensions are 46 Å × 44 Å × 38 Å of domain 1 and 32 Å × 24 Å × 22 Å of domain 2. The two domains are connected by four peptide segments, and one adenosine site is located in a cleft between the two domains. Domain 2 appears to form a flap that folds back over the adenosine substrate, shielding it from solvent.

Domain 1 includes residues 1−12, 66−116, and 142−345. The fold contains a central nine-stranded predominantly parallel β-sheet with strand order β6-β5-β1-β9-β10-β11-β12-β13-β14, where strand β13 is the only antiparallel strand (Figure 3). The β-sheet is flanked by 10 α-helices (helices α3−α12) of which eight are approximately parallel to the strands of the β-sheet. This motif forms the core of the overall AK structure. The C-terminus of the structure shows an antiparallel coiled-coil structure consisting of two α-helices (α11 and α12) joined by a short loop which runs from residue 310 to 316. Domain 2 includes residues 17−61 and 122−137. The fold contains a five-stranded mixed β-sheet flanked by two α-helices on the solvent exposed side (Figure 3). The β-sheet topology is β3-β8-β7-β2-β4. The two α-helices (α1 and α2) run approximately perpendicular to the strands of the β-sheet.

*Interaction between the Domains*. Domains 1 and 2 are connected by four peptide segments (residues 14−16, 62−65, 117−121, and 138−141). One of these regions contains Ala 139 which is an outlier in the Ramachandran plot. The folding of domain 2 over domain 1 creates the active-site cavity, and the interactions between these domains are stabilized by one of the bound adenosine molecules. The total buried surface area at the interface between domain 1 and domain 2 is 1432 Å$^2$. The presence of a Ala139 with unusual $\phi,\psi$ values and the overall folding of the 117−121 and 138−141 loops suggest a hinge type of motion around these connecting peptides.

*Adenosine Binding Sites*. There are two adenosine binding sites in the structure. Both of the adenosine molecules are well-defined (Figure 2) with average thermal parameters of 9.2 Å$^2$ for adenosine 1 and 11.6 Å$^2$ for adenosine 2. The adenosine-binding regions are illustrated in Figure 4. The adenine base of adenosine 1 is completely buried in a hydrophobic pocket formed at the intersection of the two domains while the base of adenosine 2 is partially exposed to solvent. Adenosine 1 forms hydrophobic contacts with Leu16, Leu40, Leu134, Ala136, Leu138, Phe170, and Phe201. The latter contact entails parallel stacking of the aromatic ring of Phe170 and the six-membered ring in adenosine 1. In contrast, the purine base of adenosine 2 is involved in only three hydrophobic interactions (Val284, Ile292, and Ile331).

Both adenosine molecules assume a standard anti conformation with glycosidic torsion angles of −123.3 and −165.4° for adenosines 1 and 2, respectively. However, while the ribose ring of adenosine 2 adopts a common C3′-endo conformation, the ribose rings of adenosine 1 adopt an unusual O4′-endo conformation. The ribose rings of adenosine 1 and adenosine 2 form six and four hydrogen bonds, respectively (Figure 4 and Table 4). All the hydrogen-bonding interactions with the ribose of adenosine 2 are through solvent water molecules. On the other hand, the ribose ring of adenosine 1 directly interacts with the protein. Both O2′ and O3′ are involved in two hydrogen bonds each. These interactions, which involve Asp18, hold the ribose ring rigidly in place.

*Magnesium Binding Sites*. Three tightly bound $Mg^{2+}$ ions were built into the model based on the presence of 0.16 M $MgCl_2$ in the crystallization solution, the coordination geometry for each site and the refined *B* factors. The first $Mg^{2+}$ ion (Figure 5a) is found in a channel running between the two adenosine sites where it connects the two adenosine molecules through a network of hydrogen-bonding interactions involving several water molecules. Five of the six coordinated water molecules directly interact with the protein. Two of the water molecules are involved in hydrogen bonds with the carboxylate group of Glu226. An additional water molecule bridges O5′ of adenosine 1 and the side-chain carboxamido group of Gln38 (Figure 4). The $Mg^{2+}$ ion employs one of its coordinated water molecules (W597) for bridging interactions with adenosine 2. The second $Mg^{2+}$ ion (Figure 5b) is involved in direct interaction with the protein through the side chains of Asp130 and Asn131. This $Mg^{2+}$ is approximately 17 Å away from the first $Mg^{2+}$ and is connected to the N6 atom of adenosine 2 through a series of water molecules. One of the coordinated water molecules is also involved in an interaction with Asn36 through a bridging water molecule. The third $Mg^{2+}$ ion (Figure 5c) is coordinated to Ser32 and is located on the surface of the protein. It is also involved in crystal-packing interactions. The rest of the coordination sites for both the second and third $Mg^{2+}$ ions are filled by water molecules.

*Crystal-Packing Interactions*. Each of the AK molecules makes direct packing contacts (<3.5 Å) with eight other symmetry related molecules. There are two crystallographic contacts related by a 2-fold axis. The first 2-fold axis brings Glu42 into close proximity (2.6 Å) to the same residue in the symmtery related molecule, $(1 - x, -y, z)$. The second 2-fold axis relates two His184 residues $(2 - x, -x, z)$ with a separation of 3.3 Å. The interaction along the first 2-fold is extensive spanning approximately 37 Å in length, running parallel to the crystallographic *a*-axis.

## DISCUSSION

The structure of human AK is the second example of a new family of carbohydrate kinases (*30*) and represents the first three-dimensional structure of a purine nucleoside kinase. Previously, only one other structure of a nucleoside kinase was reported [thymine kinase (*49*)], whereas four nucleotide kinase structures are known [adenylate kinase (*50*), guanylate kinase (*51*), uridylate kinase (PDB code: 1UKZ) and nucleoside diphosphate kinase (*52*)]. The overall topology of AK shows little similarity to these structures. A general feature of the nucleoside monophosphate kinase structures is the presence of a five-stranded parallel β-sheet and a characteristic P-loop. Neither AK nor thymine kinase structures exhibit these features. The arrangement of the α-helices in AK is also very different from the other


FIGURE 3: (Top) Ribbon diagram of AK including two bound adenosine molecules. The α-helices are labeled α1 through α12 and the *β*-strands are labeled *β*1−*β*14. The figure was drawn with MOLSCRIPT (47). (Bottom) Topology diagram of AK.

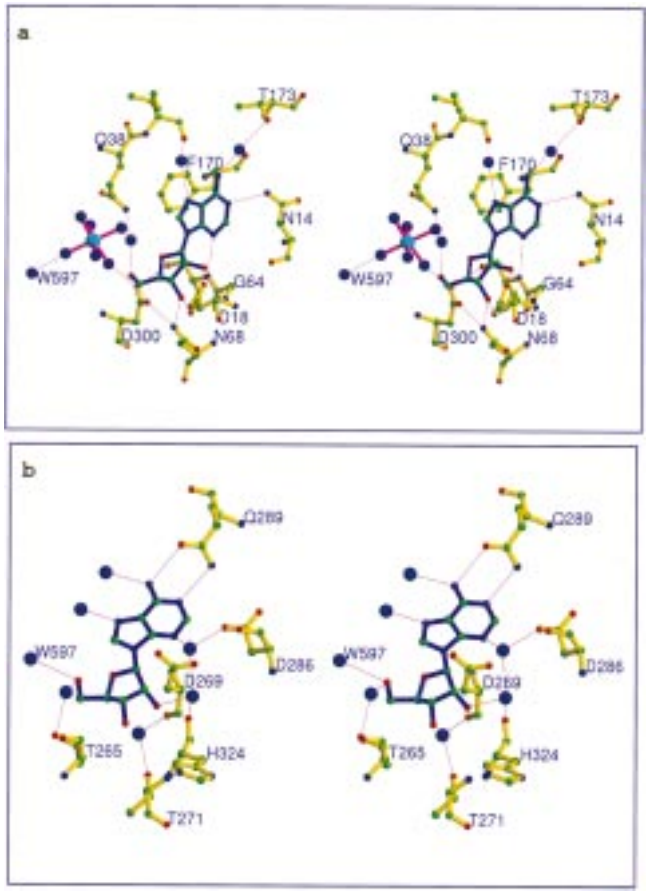


FIGURE 4: (a) Stereodrawing of the adenosine 1 binding site. (b) Stereodrawing of the adenosine 2 binding site. Amino acid residues are labeled with the one letter amino acid code.

Table 4: Hydrogen Bonds and Close Contacts Involving Adenosine (<3.5 Å)

| adenosine 1 | | | adenosine 2 | | |
|---|---|---|---|---|---|
| N1 | Asn14 ND2 | 3.12 | N1 | Gln289 NE2 | 3.05 |
| N1 | Phe170 CB | 3.42 | C2 | Asp286 O | 3.38 |
| N1 | Phe170 CG | 3.44 | N3 | W425 | 2.88 |
| N3 | Ser65 N | 3.20 | C4 | Ile331 CD1 | 3.49 |
| C6 | Phe170 CD2 | 3.46 | N6 | Gln289 OE1 | 2.99 |
| N6 | Phe170 CD2 | 3.40 | N6 | W577 | 2.76 |
| N6 | W415 | 3.28 | N7 | W637 | 2.73 |
| N6 | W416 | 3.07 | C2′ | Gly267 O | 3.38 |
| N7 | W415 | 2.85 | C3′ | Gly267 O | 3.40 |
| O2′ | Asp18 OD1 | 2.72 | O2′ | His324 CD2 | 3.47 |
| O2′ | Gly64 N | 3.13 | O2′ | W408 | 2.76 |
| O3′ | Asp18 OD2 | 2.86 | O3′ | W410 | 2.81 |
| O3′ | Gly64 N | 3.29 | O4′ | Ala327 CB | 3.48 |
| O3′ | Asn68 ND2 | 3.11 | O5′ | W420 | 2.71 |
| O4′ | W430 | 3.04 | O5′ | W597 | 2.99 |
| O5′ | Asp300 OD2 | 2.79 | | | |
| O5′ | W430 | 2.75 | | | |

nucleoside and nucleotide kinases. Sequence homology searches using the BLAST program failed to identify any sequence similarity of AK with other nucleoside or nucleotide kinases. Interestingly, this search showed sequence similarity of AK with some members of the ribokinase family. This similarity was also reported earlier (*18*, *53*).

*Structural Similarity to E. coli Ribokinase*. Evidence for high structural similarity between human AK and ribokinase (RK) is apparent by comparing the AK structure with the recently reported structure of *E. coli* RK (*30*). A search with the program DALI (*54*) revealed no additional homologous

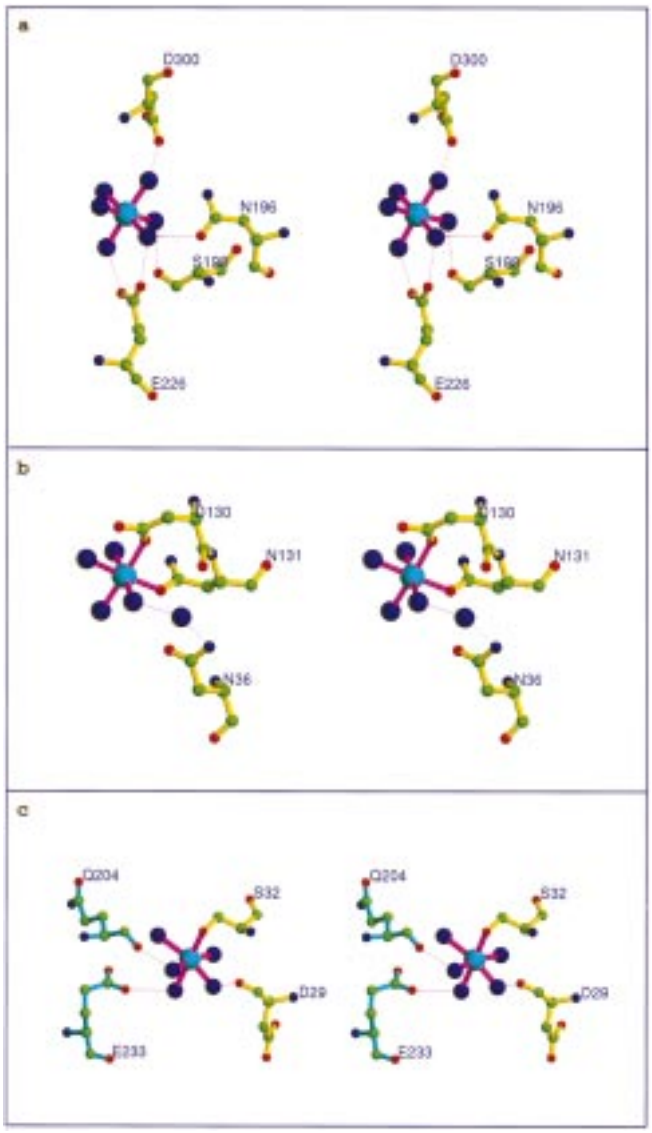


FIGURE 5: Stereoviews of the proposed Mg ion sites. (a) $Mg^{2+}$ ion 1 located near the active site. (b) $Mg^{2+}$ ion 2. (c) $Mg^{2+}$ ion 3. This figure was drawn with RIBBONS (*48*).

structures. Human AK and *E. coli* RK superimpose (Figure 6a) with an RMS deviation of 2.4 Å for 306 residues, even though the sequence identity between them is only 22%.

This comparison shows that nine $\beta$-strands of domain 1 are conserved whereas RK lacks one $\beta$-strand and the two $\alpha$-helices (*30*) found in domain 2 of AK (Figure 6b). Instead, RK forms a dimeric structure utilizing the $\beta$-sheet of domain 2 for the dimer interface. AK maintains the same domain 2 topology as RK by including an additional $\beta$-strand ($\beta$3) in the smaller domain. When the AK and RK structures are superimposed, the ribose ligand of RK (*30*) superimposes on the ribosyl group of adenosine 1 (Figure 7a) and the adenosine portion of the ADP ligand in RK superimposes on adenosine 2 (Figure 7b). This comparison provides strong evidence that adenosine 1 exists in the binding site used for the nucleoside undergoing phosphorylation and that adenosine 2 occupies the ATP/ADP-binding site. The residues involved in substrate binding derived from the comparison of the AK and RK structures are given in Table 5. A schematic representation of the substrate-binding sites derived

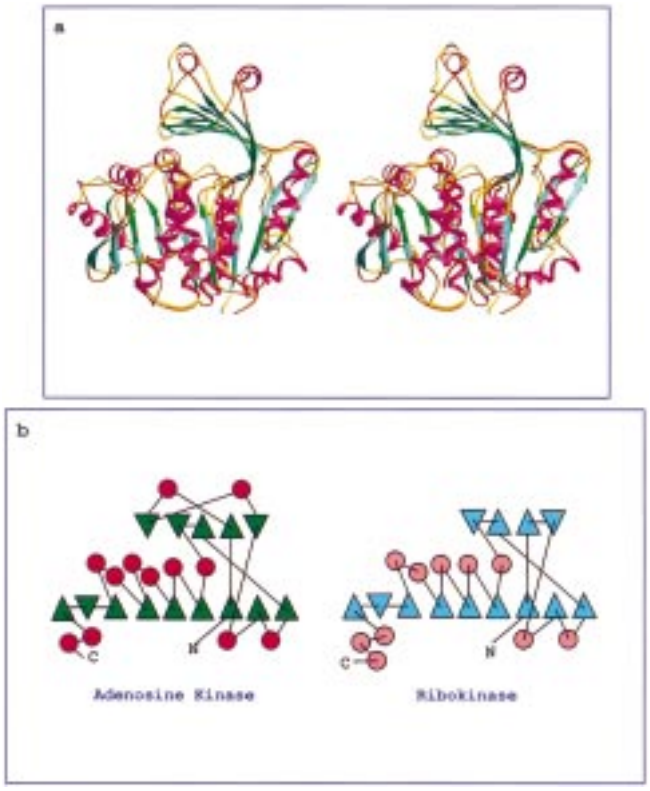


FIGURE 6: (a) Stereoview of the superposition of the AK and RK structures. (b) Topology diagrams of AK and RK; α helices are represented as circles, β strands as triangles.

from the comparison of AK and RK structures is shown in Figure 8.

The adenine base of both adenosine 2 in AK and the ADP in RK (*30*) are relatively open to the solvent. Most of the protein interactions represent hydrophobic contacts. As in the case of AK, the adenine base of RK shows close contacts with the main-chain atoms (Gly225 and Ser226). The glycine residue involved in this interaction is a well-conserved residue among various members of this new kinase family (Figure 9). The residues involved in ribose binding are also well conserved. Phe302 of AK and Phe257 in RK (*30*) are involved in hydrophobic contacts and are absolutely conserved in this kinase family. Further analysis shows that this phenylalanine residue is a part of a larger hydrophobic cluster involving at least 16 residues.

Other residues involved in the ATP/ADP-binding are also conserved among the family (Figure 9). These residues are Asn196, Asn223, Glu226, Thr265, and Gly267 in AK and Asn166, Asn187, Glu190, Thr223, and Gly225 in RK (*30*). The residues from Asn223 to Glu226 are absolutely conserved between the structures of human AK and *E. coli* RK and also show similarity among the other members. Both of the oxygen atoms of Glu226 are involved in coordinating the $Mg^{2+}$ ion in AK. The Asn196 of AK which interacts with the $Mg^{2+}$ is also conserved among the family. In RK, Asn108 from the smaller domain occupies the vicinity of the Asn196 in AK (*30*). The purine ring of adenosine 2 makes five hydrogen-bonding interactions. Even though two of these interactions are with the protein, the absence of a main-chain hydrogen-bonding interaction is noteworthy (Figures 4 and 7).

Examination of the structures of the adenosine 1 binding site of AK and the ribose binding site of RK (*30*) revealed

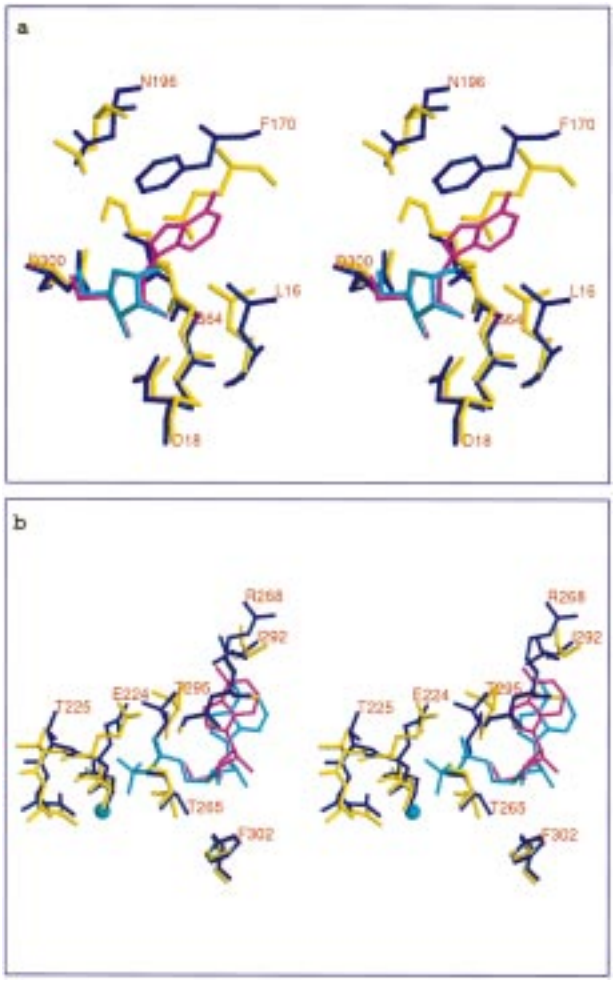


FIGURE 7: Stereoview of the superposition of the AK (blue) and RK (yellow) active site region. The AK ligands are shown in violet and the RK ligands are shown in cyan. Key AK residues are numbered. (a) Adenosine 2 binding site. (b) Adenosine 1 binding site. This figure was drawn with RIBBONS (*48*).

several similarities. As in the case of AK, the ribose of RK is deeply buried and involved in many interactions with the protein. Gly63 and Gly64 (Gly41 and Gly42 of RK), Asp18 (Asp16 in RK), and Asn68 (Asn46 in RK) all show conservation within this kinase family. From a structural point of view, the residues in RK that favor ribose binding over adenosine are Ile112, Asn14, and Glu143. In AK, Ile112 is replaced by Ala136 allowing more room for the nucleoside substrate, Asn14 is replaced by Leu16, which forms part of the hydrophobic pocket for the purine base, and Glu143 is replaced by Phe170, which is involved in strong stacking interaction with the adenine base. In addition to the hydrophobic interactions, the purine base of adenosine 1 forms four hydrogen-bonding interactions. One of these is through the side chain of Asn14, one is through a main-chain amide (G64), while the remaining two are through water molecules (Figures 4 and 7). In AK, Asp300 bridges the $Mg^{2+}$ and the O5′ atom of adenosine 1 (i.e., the atom to be phosphorylated). The corresponding residue in RK is Asp255 and is hydrogen bonded to O5′ of the ribose moiety even though the $Mg^{2+}$ ion is absent (*30*). The sequence in the vicinity of this residue, DxN(T/I)G(A)AGDxF, is very well conserved among all members of the family.

*Adenosine-Binding Site*. The assignment of the site occupied by adenosine 1 as the site occupied by the substrate

Table 5: Interacting Residues of Protein and the Ligands

| site | AK residue | RK residue | contact site | contact type |
|---|---|---|---|---|
| ATP | Gly267 | Gly225 | adenine | hydrophobic |
| | Arg268 | Ser226 | adenine | hydrophobic |
| | Asp286 | Arg243 | adenine | van der Waals |
| | Ile292 | Ala247 | adenine | hydrophobic |
| | Thr295 | Thr250 | adenine | hydrophobic |
| | Ile331 | Val286 | adenine | hydrophobic |
| | Phe302 | Phe257 | ribose | hydrophobic |
| | His324 | His279 | ribose | hydrophobic/AK H-bonding/RK |
| | Ala327 | Ala282 | ribose | hydrophobic |
| | Asn223 | Asn187 | $PO_4$ | H-bonding |
| | Thr265 | Thr223 | $PO_4$ | H-bonding |
| | Thr225 | Thr189 | $PO_4$ through water | H-bonding |
| | Glu224 | Glu188 | (near $PO_4$) | nonspecific |
| | Glu226 | Glu190 | Mg | H-bonding |
| adenosine | Asn14 | | adenine | H-bonding |
| | Ala136 | | adenine | hydrophobic |
| | Leu16 | Asn14 | adenine | hydrophobic/AK |
| | | | ribose | H-bonding/RK |
| | Ser65 | Lys43 | adenine | H-bonding/AK |
| | | | ribose | H-bonding/RK |
| | Phe170 | Glu143 | adenine | hydrophobic/AK |
| | | | ribose | H-bonding/RK |
| | Asp18 | Asp16 | ribose | H-bonding |
| | Gly63 | Gly41 | ribose | |
| | Gly64 | Gly42 | ribose | |
| | Asn68 | Asn46 | ribose | H-bonding |
| | | Ile100 | ribose | hydrophobic |
| | Leu134 | Ile110 | ribose | hydrophobic |
| | Cys123 | | ribose | van der Waals |
| | | Ile251 | ribose | hydrophobic |
| | Asp300 | Asp255 | ribose | H-bonding |

undergoing phosphorylation is based on analysis of the AK and RK structures and finding that the adenosine 1 binding site closely corresponds with the ribose-binding site in RK (*30*). In addition, adenosine 1 is in a deeply buried cavity surrounded by residues such as Asp300 expected to participate in substrate binding and catalysis. The adenosine 1 binding site is covered by the small domain and shielded from the solvent. Finally, adenosine 1 is positioned to easily accommodate direct phosphorylation by ATP in the ternary complex.

Adenosine 1 has a glycosidic torsion angle of −123.3° and O4′-endo sugar pucker. The sugar pucker is somewhat unusual compared to the more normal C2′-endo or C3′-endo conformation typically observed for purine nucleosides. The glycosidic torsion angle falls in the −anticlinal conformation. Most purine nucleosides have anti conformations for the glycosidic torsion angle and the −anticlinal conformation is consistent with the O4′-endo sugar pucker. The C4′-C5′ torsion angle is approximately in the gauche, trans conformation which extends O5′ away from the sugar ring, making it available for interactions with Asp300 and the terminal phosphate of ATP (see below).

Adenosine 1 binding is stabilized by several key interactions (Table 4). The phenyl group of Phe170 forms a stacking interaction with the purine base. The interaction with adenosine N6 is mediated by a water molecule that bridges to Thr173, and the interaction with N7 is mediated by a water that bridges to the backbone carbonyl oxygen of Ile39. The side chain of Asn14 donates a hydrogen bond to adenosine N1 and the backbone amide of Ser65 donates a hydrogen bond to adenosine N3. The remaining contacts with the purine ring are mostly hydrophobic. All three hydroxyl groups of the ribose ring are involved in multiple hydrogen bond contacts. The O2′ hydroxyl donates a hydrogen bond to Asp18 and accepts a hydrogen bond from the backbone amide of Gly64. The O3′ hydroxyl donates a hydrogen bond to Asp18 and accepts a hydrogen bond from the side chain of Asn68. The O5′ hydroxyl donates a hydrogen bond to Asp300 and accepts a hydrogen bond from a water molecule. This water molecule forms a hydrogen bond to another water molecule, which is part of the $Mg^{2+}$ ion coordination sphere.

The mode of adenosine binding in AK is somewhat unique compared to other adenosine-binding enzymes. This may be in part due to the requirement that the O5′ hydroxyl group be free to participate in the catalytic reaction while providing some specificity for adenosine as the purine base. In most enzymes that bind purine nucleosides, an aromatic side chain packs against one face of the purine base. However, other adenosine-binding enzymes use primarily side-chain or main-chain atoms to form hydrogen bonds with atoms on the edge of the purine ring. In RK, where the adenine base is absent, the active site adapts to the smaller substrate, ribose, by reducing the active-site volume though side-chain substitutions and amino acid insertions (Figure 7a). On the other hand, residues involved in ribose binding are conserved across AK and RK and among the AKs from various species (Figure 9). These residues include Asp18, Gly64, Asn68, and Asp300.

*ATP Binding Site*. The assignment of adenosine 2 to the ATP-binding site is based in large part on the finding that the adenosine 2 site closely overlaps the ADP site in RK (*30*) when the two protein active structures are superimposed (Figure 7b). Furthermore, model building suggests that the spacing between the two adenosine sites is suitable for direct phosphorylation of adenosine by ATP. The modeling studies suggest that ATP stretches out along the edge of the central $\beta$-sheet in the trough between the two adenosine-binding sites. The trough also contains one of the three $Mg^{2+}$ ion sites observed in the crystal structure of human AK. The homology between AK and RK with ADP and ribose bound and the geometric requirements for the catalytic reaction provide convincing evidence that adenosine 2 occupies the ATP-binding site. In addition, the kinetic data for the human erythrocytic enzyme suggested a second adenosine-binding site with significantly lower binding affinity than the catalytic site (*23*, *28*). On the basis of the X-ray structure, adenosine 1 is expected to occupy the higher affinity binding site since adenosine 2 is located closer to the surface of the protein. Furthermore, adenosine 2 is surrounded by water molecules and only directly interacts with AK through hydrogen bonds with Gln289 at N1 and N6. Last, finding adenosine 2 in the ATP-binding site is consistent with studies suggesting that adenosine is a competitive inhibitor of ATP.

Another structural feature of the adenosine 2 binding site suggesting that it is the ATP binding site is the finding of a $Mg^{2+}$ ion nearby. Modeling an ATP molecule in the adenosine 2 site suggests that $Mg^{2+}$ is in a position to interact with the $\beta$- and $\gamma$-phosphate groups. Although this is supportive data, it should be noted that the crystals were grown in the presence of 0.16 M $Mg^{2+}$ ion and the $Mg^{2+}$ site may be an artifact. Accordingly, two other $Mg^{2+}$ ion

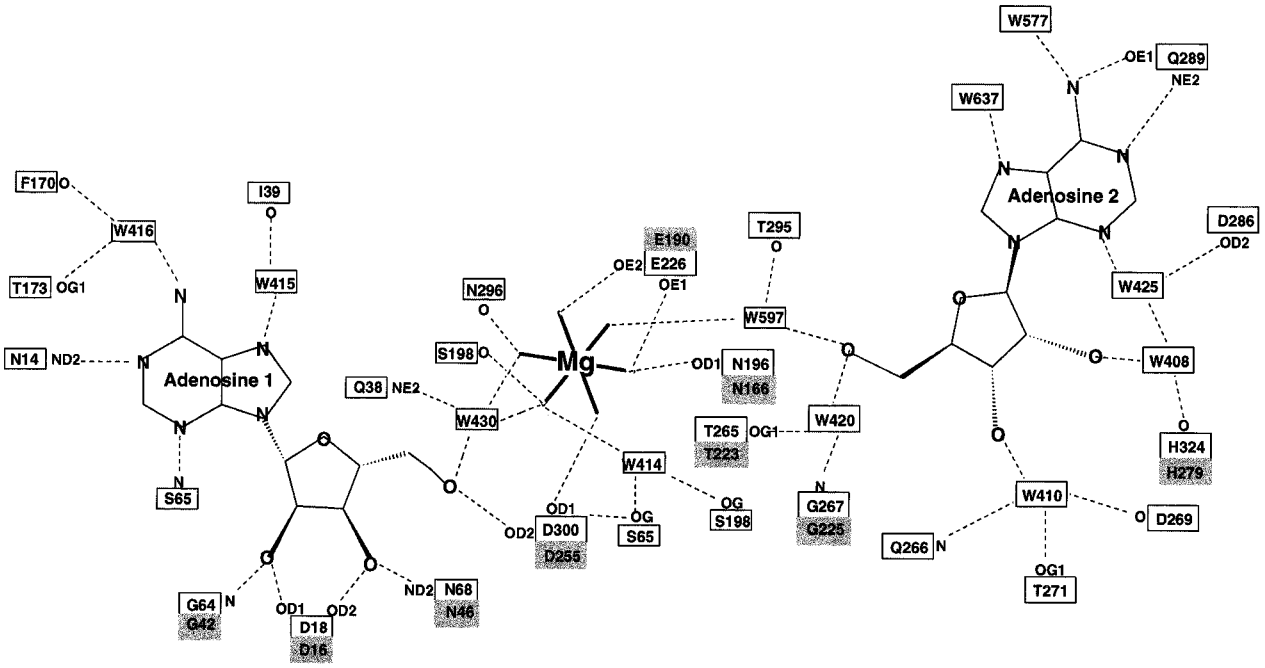


FIGURE 8: Schematic drawing showing the relationship of the ATP and adenosine/ribose binding sites for AK and RK. AK residues are shown in unshaded boxes and corresponding RK residues are shown in shaded boxes. Amino acid residues are labeled with the one letter amino acid code.

sites were observed for which no structural or mechanistic role is apparent. Nevertheless, based on other kinases and the requirement of $Mg^{2+}$ for catalytic activity, the $Mg^{2+}$ ion is likely involved in orienting the terminal ATP phosphate and stabilizing the phosphate during transfer to adenosine. One of the residues involved in $Mg^{2+}$ ion binding (Ser198) is an outlier in the Ramachandran plot.

Analysis of other proteins complexed with GTP or ATP and $Mg^{2+}$ suggest that $Mg^{2+}$ is usually coordinated to an Asp residue directly or through a water molecule (*49*, *56*−*59*). In the case of p21 *ras* $Mg^{2+}$−ATP complex, the water-mediated coordination of Asp57 to $Mg^{2+}$ shifts to direct coordination upon hydrolysis to ADP (*60*). In the present structure, while one of the Asp300 oxygen atoms (OD1, Figure 8) coordinates to $Mg^{2+}$ through a water molecule, the other oxygen atom (OD2) coordinates to O5′ of adenosine 1. The sequence near this Asp residue is DTNGAGDAF (residues 294−302). Sequence homology searches of AK using the BLAST program showed the presence of similar sequence in all adenosine kinases, ribokinase, fructokinase, deoxygluconokinase, guanosine kinase, and inosine-guanosine kinase, with a consensus sequence DT(A,S,P)T(N,I)G-(A)AGD. Out of the 35 or so different sequences, 26 have the conserved DT-GAGD sequence motif. In the case of inosine-guanosine kinase, the first aspartate residue is replaced by an asparagine residue. A secondary structure prediction (*61*) with members of the family shows the presence of this sequence at the start of an α-helix. Similarly, this sequence also occurs in the beginning of α-helix 12 (residues 294−311) in AK. The consensus sequence also contains Asp300 residue of AK which corresponds to Asp255 in RK.

Both N1 and N6 of adenosine 2 are involved in hydrogen-bonding interactions with OE1 and NE2 of Gln289, respectively. The substitution of carbonyl at the N6 position in a guanine ring would still allow for these hydrogen bonds after a 180° rotation of the CG−CD bond, leading to the NE2−carbonyl (guanine) interaction and the OE1−N1 (guanine) interaction. This is consistent with the finding that AK can also use GTP as the phosphate donor in the kinase reaction but does not necessarily account for the fact that GTP is preferred by AK over ATP as a phosphate donor (*3*).

*Spatial Analysis of the Adenosine 1 and Adenosine 2 Binding Sites*. Additional support for the interpretation of the adenosine-binding sites comes from consideration of their spatial arrangement (Figures 10 and 11). Crystal structural studies with bisubstrate analogues have helped delineate the pathway for phosphoryl transfer in adenylate kinase (*50*). Similarly, the bisubstrate analogue P1,P4-(diadenosine 5′)-tetraphosphate (Ap4A) is a potent AK inhibitor with a $K_d$ of 30 nM (*62*). Strongest inhibition was achieved in compounds containing four or five phosphoryl groups linking the two adenosine moeities. This spacer link corresponds to one or two more phosphoryl groups than provided by substates, ATP, and adenosine or ADP and AMP. These results are similar to findings reported for adenylate kinase and thymidylate kinase and suggest a direct transfer of the phosphoryl group from ATP to the acceptor. Furthermore, these results are supported by modeling studies which suggest that four phosphates are optimal for bridging the two adenosine sites of AK (Figures 10 and 11). This brings the sequence NGAG (residues 296−299) close to the phosphate groups. The relative position of $Mg^{2+}$ with respect to phosphates and adenosine is very close to that observed in other structures (*56*, *57*). However, the absence of basic side chains near this site is noteworthy. The ribokinase has one lysine residue (Lys143) pointing to the active site. This might indicate a conformational change in the enzyme during ATP binding (*29*), which would bring basic side chains into the vicinity of the phosphate. The basic side chains in the vicinity of the AK active site are Arg132 and Arg268. Among these residues, Arg132 is absolutely conserved among the kinase

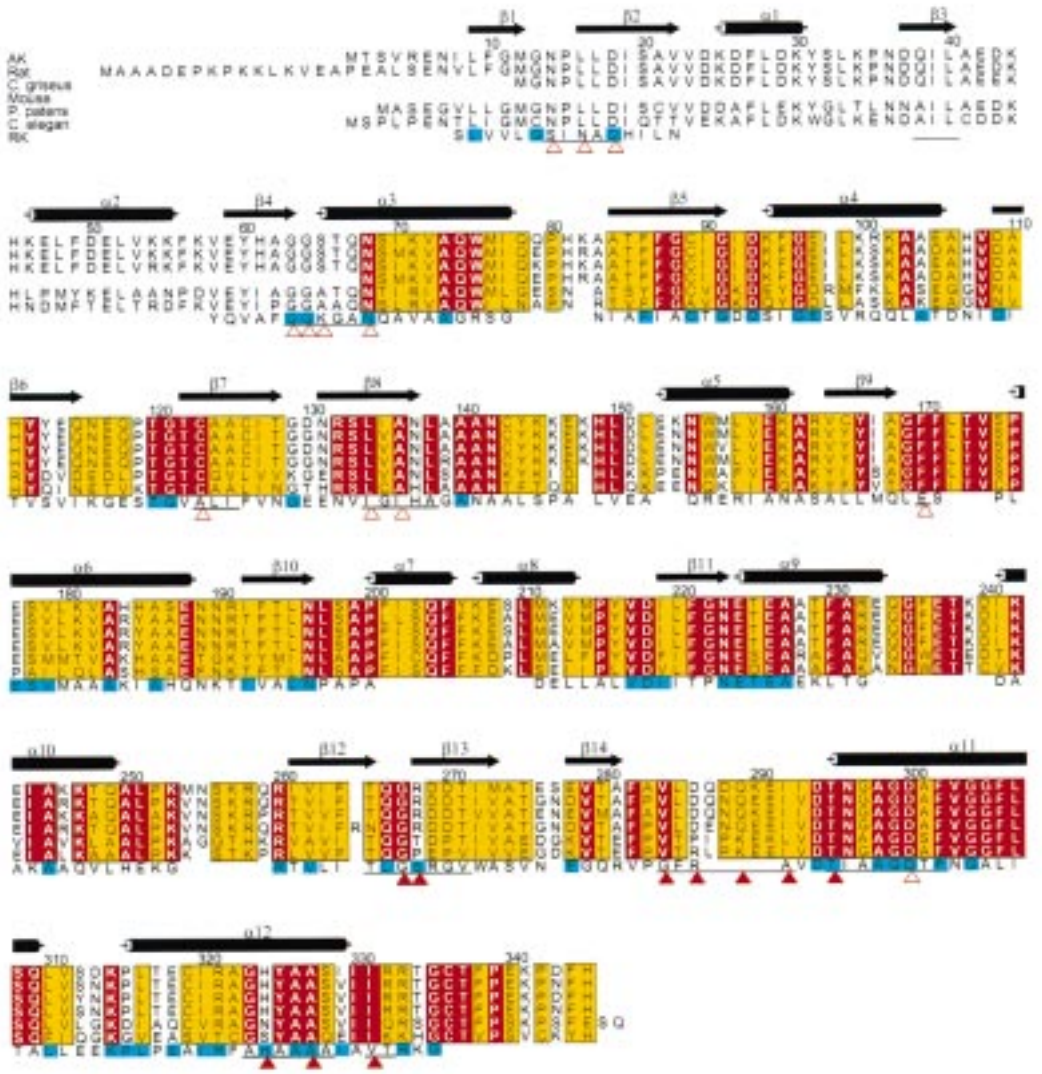

FIGURE 9: Sequence comparisons of AK from different organisms and *E. coli* RK. Numbering follows the sequence of AK for which secondary structures are shown as cylinders (helices) and arrows (strands). Identities among all AK sequence are shown with red backgrounds, positions at which amino acids with similar physical-chemical properties are conserved are shown in yellow. The alignment of AK and RK is derived from the three-dimensional structure comparison. Identical residues in both AK and RK are shown in cyan in the RK sequence. Residues involved in interactions (hydrophobic and/or hydrogen bonding) with adenosine 1 and adenosine 2 are shown by open and filled triangles, respectively. Residues near the adenosine binding region are underlined. GenBank accession numbers for the various AK sequences are rat (U90340), *Cricetulus griseus* (P55262), Mouse (P55264), *Physcommitrella patens* (Y15430), and *Caenorhabditis elegan* (Z81107). The figure was drawn with ALSCRIPT (*55*).

family. Furthermore, a torsional rotation of the Arg132 side chain of AK brings the NH1 close to the $Mg^{2+}$ ion (6.1 Å). The distance between the basic side chain in the active site of RK (Lys43 NZ) and the catalytic $Mg^{2+}$ ion in AK is 5.3 Å.

*Substrate Binding and Catalytic Mechanism*. The AK structure and the postulated model of the AK−Ado−ATP ternary complex (Figures 10 and 11) are consistent with many of the results reported in earlier kinetic studies. For example, saturation kinetics suggested that AK had two adenosine-binding sites and that adenosine binding to the low-affinity site was responsible for the decreased enzymatic activity observed at high substrate concentration (*25*). Our studies confirm the presence of both binding sites and suggest that the substrate inhibition is due to competitive inhibition of ATP binding. It should be noted, however, that the latter conclusion is inconsistent with other kinetic data showing adenosine to be a noncompetitive inhibitor of ATP binding (*21*)[1] and with conclusions drawn from DTNB inactivation studies suggesting that the ATP-binding site is distinct from the two adenosine sites (*23*). These conclusions were based primarily on the failure of ATP to inhibit AK inactivation by DTNB, whereas inactivation was prevented by adenosine but only at concentrations an order of magnitude greater than the estimated dissociation constant for adenosine at the catalytic site. Accordingly, the authors postulated that AK inactivation occurred via alkylation of a cysteine sulfhydryl located at the low-affinity adenosine-binding site. The X-ray structure, however, shows a cysteine residue near the adenosine 1 binding site (Cys123) and no cysteine near adenosine 2. These results and the model of the ternary complex, therefore, are consistent with the inactivation study

[1] Kinetic studies using the recombinant human enzyme show competitive inhibition kinetics (D. Dumas, unpublished results). The reasons for the apparent discrepancy in results are unclear.

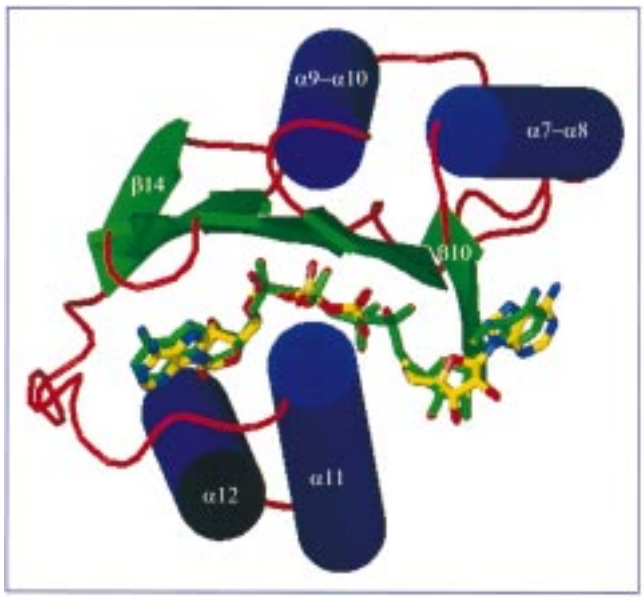


FIGURE 10: Schematic diagram showing the modeled ATP and adenosine in red and yellow and modeled Ap4A in purple.

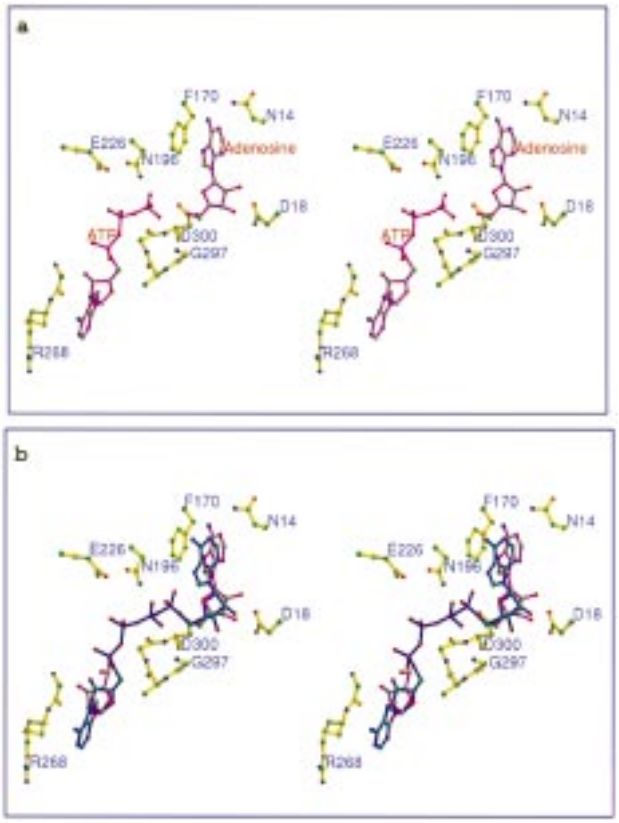


FIGURE 11: Stereodiagram showing key active site residues and modeled (a) ATP and (b) Ap4A binding sites.

results but suggest that adenosine bound to the catalytic site is responsible for the observed protection of AK from DTNB inactivation.

The postulated model of the ternary complex is also consistent with an ordered bi-bi kinetic mechanism. The model ruled out a ping-pong mechanism since no residue is in the vicinity of the active site that could act as a phosphate acceptor. In contrast, the model indicated that the 5′-hydroxyl of adenosine is near the $\gamma$-phosphate of ATP and in reasonable alignment with the $\gamma$-phosphate to suggest an

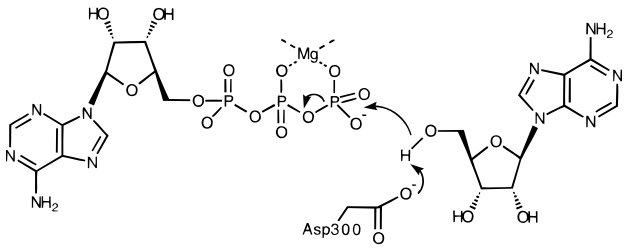


FIGURE 12: Catalytic mechanism of AK showing the proposed orientation of adenosine and illustrating the role of Asp300 in deprotonation of the adenosine 5′-hydroxyl group. (1) Kinetic studies using the recombinant human enzyme show competitive inhibition kinetics (D. Dumas, unpublished results). The reasons for the apparent discrepancy in results are unclear. (2) Tryptophan fluorescent studies suggest that ATP binding, but not adenosine binding, produces fluorescence quenching and decreased accessibility to acrylamide and iodide (*29*). Without the X-ray structure of the AK−ATP complex, it is unclear whether these results suggest a substantial protein conformational change and a different geometrical relationship between the adenosine and ATP-binding sites.

in-line $S_N2$ displacement reaction.[2] The model also provided some possible insight into the preferred order of substrate binding and product release. Since the adenosine 1 binding site is significantly more buried and further from the solvent interface than adenosine 2, it seems reasonable to postulate that, without invoking a protein conformational change, adenosine binds prior to ATP. This is consistent with most of the earlier kinetic studies (*21*−*24*) but not all (*20*).

Analysis of the AK X-ray structure and ternary complex model also provided some insight into the catalytic mechanism. As with other kinases, $Mg^{2+}$ is located at a position relative to the postulated positions of the ATP $\beta$- and $\gamma$-phosphates to simultaneously coordinate with both and thereby decrease negative charge and enhance the leaving group ability of ADP (Figure 12). In the model, the 5′-hydroxyl of adenosine is 4.4 Å from the $\gamma$-phosphate and in position for an $S_N2$-type displacement as inferred from mechanistic studies showing that AK proceeded with inversion of configuration at the $\gamma$-phosphate (*19*). The 5′-hydroxyl is also near the carboxylate of Asp300, suggesting that the carboxylate is the catalytic base that deprotonates the hydroxyl prior to attack on the $\gamma$-phosphate (Figure 12). Data supporting Asp300 as a catalytic base includes the presence of Asp255 in ribose kinase at a similar geometrical position (*30*) and the large decrease in catalytic activity at pH values below 5.5 (*21*). Use of carboxylate groups as active-site bases for deprotonation of hydroxyl groups is well precedented (*63*).

*Structure*−*Activity Relationships*. An analysis of the protein residue contacts with adenosine and the reported AK substrate specificity (*3*) further supported the adenosine 1 binding site as the catalytic site responsible for binding the nucleoside substrate. For example, AK catalyzes the phosphorylation of adenosine analogues with a purine base specificity of purine ≈ 8-azapurine > 7-deazapurine ≈ 7-deaza-8-azapurine > 1-deazapurine ≫ 3-deazapurine. The

[2] Tryptophan fluorescent studies suggest that ATP binding, but not adenosine binding, produces fluorescence quenching and decreased accessibility to acrylamide and iodide (*29*). Without the X-ray structure of the AK-ATP complex, it is unclear whether these results suggest a substantial protein conformational change and a different geomertrical relationship between the adenosine and ATP-binding sites.

poor activity of 1-deaza analogues and the absence of binding detected for 3-deaza analogues is consistent with the crystallographic data, indicating that both nitrogen atoms accept a hydrogen bond from AK. The failure of 3-deaza analogues to bind is attributed to the use of a backbone NH as the hydrogen bond donor, which in comparison to the hydrogen bond, donated by the carboxamido group of Gln289 to N1 is held relatively rigid in space and therefore forms a stronger hydrogen bond with little ability to accommodate replacement of the ring nitrogen with −CH. In contrast, base modifications at the 7- and 8-positions have less of an effect on catalytic activity. The X-ray structure is consistent with these findings in that no residues are near C8 and only a bridging water molecule is in hydrogen bond contact with N7. Accordingly, 7-deaza analogues are modest substrates of AK, and formycin analogues (pyrazolo[4,3-d]pyrimidines), which have an NH at N7 and therefore act as a hydrogen bond donor, are excellent substrates. The finding of a bridging water in contact with N7 may also explain the high affinity of iodotubercidin analogues (5-iodo-4-aminopyrrolopyrimidine ribofuranose), since the iodo group could displace the water molecule and gain affinity through the hydrophobic effect (*64*).

The X-ray structure is also consistent with the known AK specificity for base substituents. N1-oxides are good AK substrates which could be explained by a modest realignment of the Glu289 side chain such that the amido group donates a hydrogen bond to the oxygen. Substituents that reside at the equivalent position of N7 in adenosine are also well accommodated by AK. For example, tubercidin (4-aminopyrrolo[2,3-d]pyrimidine, i.e., 7-deazaadenosine) with an iodo, cyano (toyocomycin), or carboxamido (sangivomycin) group at this position is an excellent substrate of AK. The large loss in catalytic efficiency with 2-substituted adenosine analogues is attributed to the limited space in this region of the binding cavity (<4 Å from $\beta$-carbon of Gln289 side chain). Substituents at the 6- and 8-positions are also reported to result in decreased catalytic efficiencies. In contrast to the 2-position, the 8-position appears to have more room for substituents, thereby suggesting that the loss in activity observed with 8-substituted analogues may reflect well-known effects of 8-substituents on nucleoside conformation and not unfavorable contacts with the protein (*65*). Replacement of the 6-amino group with H, $CH_3$, Cl, and $SCH_3$ results in a 25−250-fold decrease in catalytic efficiency. The X-ray structure indicates that the amino group donates two hydrogen bonds to water. The large loss in affinity is therefore likely to reflect the simultaneous loss of two bridging water molecule interactions. The inhibitory activity of analogues with a 6-N(H)Ar is consistent with the space available to substituents near the 6-position and the expected ability of these aryl substituents to displace the water molecule and form favorable interactions with hydrophobic groups in this region of the binding site, particularly Phe170, Phe201, and a valine residue (*3*, *66*). The $10^5$-fold loss in catalytic efficiency for inosine is consistent with other nucleoside binding enzymes (*67*, *68*) and is attributed to the simultaneous loss of the N6 and N1 hydrogen bonds.

The AK X-ray structure also exhibits structural features that are consistent with the known sugar specificity of AK. In general, changes in the configuration or presence of sugar hydroxyl groups leads to a large decrease in catalytic efficiency. The order of substrate preference is reported to be ribosyl ≫ lyxofuranosyl > 3′-deoxyribosyl > xylosyl > 2′-deoxyribosyl > arabinosyl ≫ 4′-deoxyribosyl. The loss in efficiency with loss of either the 2′ or 3′ hydroxyls is attributed to the presence of Asp18, which is in position to accept hydrogen bonds from both hydroxyls. The greater importance of the 2′ hydroxyl relative to the 3′ hydroxyl may reflect the difference in hydrogen bond strength between the backbone Gly64 NH hydrogen bond with the 2′-hydroxyl and the hydrogen bond formed between the 3′ hydroxyl and the side-chain amido group of Asn68. The further decrease in activity of the xylo and arabino configurations is likely a result of a hydrophilic hydroxyl group on the $\beta$-face of the ribose, since this face is in a relatively hydrophobic environment made up of the side chains of Leu134 and Cys123. Less readily explained by the X-ray structure is the large decrease in catalytic efficiency associated with replacement of the ribosyl oxygen with a methylene (aristomycin), since the only interaction with AK is through a bridging water molecule. Possibly the loss in activity is due instead to a change in the preferred solution conformation or ring pucker which ultimately is reflected in high ligand strain in the binding conformation.

## REFERENCES


1. Snyder, F. F., and Lukey, T. (1982) *Biochim. Biophys. Acta 696*, 299−307.
2. Krenetsky, T. A., Miller, R. L., and Fyfe, J. A. (1974) *Biochem. Pharmacol. 23*, 170−172.
3. Miller, R. L., Adamczyk, D. L., Miller, W. H., Koszalka, G. W., Rideout, J. L., Beacham, L. M., III., Chao, E. Y., Haggerty, J. J., Krenitsky, T. A., and Elion, G. B. (1979) *J. Biol. Chem. 254*, 2346−2352.
4. Willis, R. C., and Carson, D. A. (1978) *Proc. Natl. Acad. Sci. U.S.A. 75*, 3042−3044.
5. Yamda, Y., Goto, H., and Ogasawara, N. (1981) *Biochim. Biophys. Acta 660*, 36−43.
6. Decking, U. K. M., Schlieper, G., Kroll, K., and Schrader, J. (1997) *Circ. Res. 81*, 154−164.
7. Schrader, J. (1990) *Circulation 81*, 389−391.
8. Erion, M. D. (1993) *Ann. Rep. Med. Chem. 28*, 295−304.
9. Miller, L. P., Jelovich, L. A., Yao, L., DaRe, J., Vgarker, B., and Foster, A. C. (1996) *Neurosci. Lett. 220*, 73−76
10. Wiesner, J. B., Zimring, S. T., Castellino, A. J., Ugarkar, B. G., Shea, M., Erion, M. D., and Foster A. C. (1995) *Epilepsia 36* (Suppl. 4), 86.
11. Keill, G. J., II, and Delander, G. E. (1994) *Eur. J. Pharmacol. 271*, 37−46.
12. Rosengren, S. G, Bong, G. W., and Firestein, G. S. (1995) *J. Immunol. 154*, 5444−5451.
13. Leibach, T. K., Spiess, G. I., Neudecker, T. J., Pesche, G. J., Puchwein, G., and Hartmann, G. R. (1971) *Hoppe-Seyler's Z. Physiol. Chem. 352*, 328−344.
14. Andres, C. M., and Fox, I. H. (1979) *J. Biol. Chem. 254*, 11388−11393.
15. Mimouni, M., Bontemps, F., and Van den Berghe, G. (1994) *J. Biol. Chem. 269*, 17820−17825.
16. Yamada, Y., Goto, H., and Ogasawara, N. (1980) *Biochim. Biophys. Acta 616*, 199−207.
17. Chang, C.-H., Cha, S., Brockman, R. W., and Bennett, L. L., Jr. (1983) *Biochemistry 22*, 600−611.
18. Spychala, J., Datta, N. S., Takabayashi, K., Datta, M., Fox, I. H., Gribbin, T., and Mitchell, B. S. (1996) *Proc. Natl. Acad. Sci. U.S.A. 93*, 1232−1237.
19. Richard, J. P., Carr, M. C., Ives, D. H., and Frey, P. A. (1980) *Biochem. Biophys. Res. Commun. 94*, 1052−1056.
20. Henderson, J. F., Mikoshiba, A., Chu. S. Y., and Caldwell, I. C. (1972) *J. Biol. Chem. 247*, 1972−1975.

21. Palella, T. D., Andres, C. M., and Fox, I. H. (1980) *J. Biol. Chem. 255*, 5264−5269.
22. Rotllan, P., and Miras Portugal, M. T. (1985) *Eur. J. Biochem. 151*, 365−371.
23. Hawkins, C. F., and Bagnara, A. S. (1987) *Biochemistry 26*, 1982−1987.
24. Bhaumik, D., and Datta, A. K. (1988) *Mol. Biochem. Parasitol. 28*, 181−187.
25. Fisher, M. N., and Newsholme, E. A. (1984) *Biochem. J. 221*, 521−528.
26. Lin, B. B., Hurley, M. C., and Fox, I. H. (1988) *Mol. Pharmacol. 34*, 501−505.
27. Neudecker, T. J., and Hartmann, G. R. (1972) *Hoppe-Seyler's Z. Physiol. Chem. 353*, 1553.
28. Neudecker, T. J., and Hartmann, G. R. (1978) *Hoppe-Seyler's Z. Physiol. Chem. 359*, 1771−1776.
29. Elalaoui, A., Divita, G., Maury, G., Imbach, J.-L., and Goody, R. S. (1994) *Eur. J. Biochem. 221*, 839−846.
30. Sigrell, J. A., Cameron, A. D., Jones, T. A., and Mowbray, S. L. (1998) *Structure 6*, 183−193.
31. Leslie, A. G. W. (1992) *Joint CCP4 and ESF-EACBM Newsletter on Protein Crystallography*, No. 26, Daresbury Laboratory, Warrington, U.K.
32. Collaborative Computational Project Number 4 (1994) *Acta Crystallogr., Sect. D 50*, 760−763.
33. Otwinowski, Z., and Minor, W. (1997) *Methods Enzymol. 276*, 307−326.
34. Blessing, R. H. (1998) *J. Appl. Crystallogr.* (in press)
35. Hendrickson, W. A., Smith, J. A., Phizackerley, R. P., and Merritt, E. A. (1988) *Proteins 4*, 77−78.
36. Hendrickson, W. A. (1991) *Science 254*, 51−58.
37. Miller, R., Gallo, S. M., Khalak, H. G., and Weeks, C. M. (1994) *J. Appl. Crystallogr. 27*, 613−621.
38. Blessing, R. H. (1997) *J. Appl. Crystallogr. 30*, 176−178.
39. Blessing, R. H., Guo, D. Y., and Langs, D. A. (1997) in *Direct Methods for Solving Macromolecular Structures. NATO ASI Series Volume* (Fortier, S., Ed.) Kluwer Academic Publishers, Dordrecht, The Netherlands (in press).
40. Terwilliger, T. C., and Berendezen, J. (1998) *Acta Crystallogr.* (in press).
41. Otwinowski, Z. (1991) *Daresbury Study Weekend Proceedings*.
42. Jones, T. A., and Kjeldgaard, M. (1993) *O version 5.9. The Manual*, Uppsala University, Uppsala, Sweden.
43. Brunger, A. T. (1996) *X-PLOR Version 3.843, a System for X-ray Crystallography and NMR*, Yale University, New Haven, CT.
44. Laskowski, R. A., MacArthur, M. W., Moss, D., and Thorton, J. M. (1993) *J. Appl. Crystallogr. 26*, 283−291.
45. Ramachandran, C., and Ramakrishnan, G. N. (1965) *Biophys. J. 5*, 909−933.
46. Luzzati, V (1952) *Acta Crystallogr. 5*, 802−810.
47. Kraulis, P. J. (1991) *J. Appl. Crystallogr. 24*, 946−950.
48. Carson, M. (1991) *J. Appl. Crystallogr. 24*, 958−961.
49. Wild, K., and Bohner, T. *Protein Sci.* (1997) *6*, 2097−2106.
50. Abele, U., and Schulz, G. E. (1995) *Protein Sci. 4*, 1262−1271.
51. Stehle, T., and Schulz, G. E. (1992) *J. Mol. Biol. 224*, 1127−1141.
52. Webb, P. A., Perisic, O., Mendola, C. E., Backer, J. M., and Williams, R. L. (1995) *J. Mol. Biol. 251*, 574−587.
53. Singh, B., Hao, W., Wu, Z., Eigl, B., and Gupta, R. S. (1996) *Eur. J. Biochem. 241*, 564−571.
54. Holm, L., and Sander, C. (1993) *J. Mol. Biol. 233*, 123−138.
55. Barton, G. J. (1993) *Protein Eng. 6*, 37−40.
56. Xu, R.-M., Carmel, G., Sweet, R. M., Kuret, J., and Cheng, X. (1995) *EMBO J. 14*, 1015−1023.
57. Tart, L. W., Matte, A., Pugazhenthi, U., Goldie, H., and Delbaere, L. T. (1996) *Nat. Struct. Biol. 3*, 355−363.
58. Pai, E. F., Krengel, U., Petsko, G. A., Goody, R. S., Kabsch, W., and Wittinghofer, A. (1990) *EMBO J. 9*, 2351−2359.
59. Story, R. M., and Steitz, T. A. (1992) *Nature 355*, 374−376.
60. Pai, E. F., Kabsch, W., Krengel, U., Holmes, K. C., John, J., and Wittinghofer, A. (1989) *Nature 341*, 209−214.
61. Rost, B. (1996) *Methods Enzymol. 266*, 525−539.
62. Bone, R., Cheng, Y.-C., and Wolfenden, R. (1986) *J. Biol. Chem. 261*, 16410−16413.
63. Pompliano, D. L., Peyman, A., and Knowles, J. R. (1990) *Biochemistry 29*, 3186−3194.
64. Davies, L. P., Jamieson, D. D., Baird-Lambert, J. A., and Kazlauskas, R. (1984) *Biochem. Pharmacol. 33*, 347−355.
65. Sarma, R. H., Lee, C. H., Evans, F. E., Yathindra, N., and Sundaralingam, M. (1974) *J. Am. Chem. Soc. 96*, 7337−7348.
66. Erion, M. D., Ugarkar, B. G., Dare, J., Castellino, A. J., Jujitaki, J. M., Dixon, R., Appleman, J. R., and Weisner, J. W. (1997) *Nucleosides Nucleotides 16*, 1013−1026.
67. Erion, M. D., Takabayashi, K., Smith H. B., Kessi, J., Wagner, S., Hönger, S., Shames, S. L., and Ealick, S. E. (1997) *Biochemistry 36*, 11725−11734.
68. Stoeckler, J. D, Poirot, A. F., Smith, R. M, Parks, R. E., Jr., Ealick, S. E., Takabayashi, K., and Erion, M. D. (1997) *Biochemistry 36*, 11749−11756.


BI9815445